SCIENTIFIC REPORTS

OPEN

A new analytical model for flow in acidized fractured-vuggy porous media

Received: 31 January 2019
Accepted: 24 May 2019
Published online: 05 June 2019

Gang Lei[1], Qinzhuo Liao[1] & Dongxiao Zhang[2]

Acidizing is one of the widely used technologies that makes the development of naturally fractured-vuggy reservoirs effective. During the process of acidizing, carbonate minerals are dissolved by hydrochloric acid, which can create high conductivity channels and wormholes to connect fractures and pores. In this work, a new analytical model, incorporating the heterogeneity of the pore networks into acidizing region, is proposed to study the flow characteristics in acidized fractured-vuggy reservoirs. The model is coupled by an acidized inner region and a conceptualized outer region of common triple medium. The porosity and permeability of inner region, which are rather heterogeneous and disordered when observed at different length scales, can be well addressed by fractal theory. The properties of the outer region can be described with three basic parameters: the matrix block size L_M, the space interval of fracture L_F and the radius of the vug L_v. Results show that the flow characteristic curves can be characterized by six flow stages (i.e. wellbore storage stage, radial flow stage in the interior region, fracture-vug inter-porosity flow stage, transition flow stage, fracture-matrix inter-porosity flow stage and external boundary response stage). It can be applied to estimate reservoir parameters for uncertainty reduction using inverse modeling.

In the past few decades, characterizing the fluid flow mechanism in fractured-vuggy porous media has become a hot topic in petroleum engineering, as increasing carbonate reservoirs are discovered worldwide[1–6]. It is reported that fractured-vuggy reservoirs have complex pore systems including matrix, fractures and vugs which cause the fluid flow characteristics within these reservoirs more complicated than that in conventional sandstones[7–11].

At present, acidizing or acid fracturing stimulation technology is essential for the development of fractured-vuggy carbonate reservoirs[12,13]. As acid is injected, carbonate minerals are dissolved and highly conductive channels or wormholes are usually formed[14]. Wormhole forming mechanism in carbonate porous media has been widely investigated using experimental and theoretical methods[15–21]. Many scholars have suggested acid flow in the pore networks selectively and create different types of wormhole structures[17,20]. Mostofizadeh and Economides[15] carried out radial acidizing tests on limestone rocks and suggested there exist an optimum injection rate. Frick *et al.*[16] conducted radial core experiments to investigate the interaction between hydrochloric acid and limestones and identified the optimum injection rate. Fredd[17] presented a dynamic mathematical model for wormhole formation determine, and suggested the derived model can be used to determining optimal acidizing strategies. Tremblay[18] proposed a sand transport model to calculate the wormhole growth. Liu *et al.*[19] derived a coupled model to study the wormhole propagation behavior under reservoir condition and they concluded that, due to the effect of the compressed zone, there existed a maximum wormhole length for both constant rate condition and constant pressure condition. Zakaria[20] conducted various laboratory tests to study the acid stimulation treatments in carbonate rocks and suggested that acid stimulation treatments are significantly affected by the pore heterogeneity and the acid propagate through the fractured-vuggy carbonate rocks in a selective manner. Li *et al.*[21] studied the moving interface of acid fingering using both the experimental tests and numerical method. Dejam *et al.*[22–27] formulated mathematical models to study the solute transport and dispersion in porous media with coupled systems. In addition, a theoretical model was derived by Ugursal[28] to evaluate acid fracturing performances in carbonate rocks.

Recently, the fluid flow and transport behavior in fractured-vuggy porous media have been analyzed with theoretical methods[3,9,29–34]. Wu *et al.*[29–31] investigated multiphase flow in fractured-vuggy reservoirs using

[1]Department of Petroleum Engineering, CPG, King Fahd University of Petroleum and Minerals, Dhahran, Saudi Arabia. [2]ERE & BIC-ESAT, College of Engineering, Peking University, Beijing, China. Correspondence and requests for materials should be addressed to Q.L. (email: qinzhuo.liao@kfupm.edu.sa)

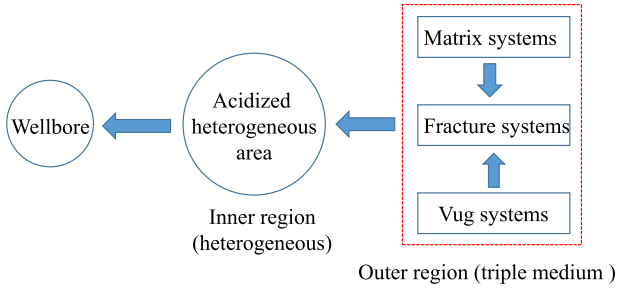

Figure 1. Schematic diagram of the physical model.

triple-continuum models. Yao *et al.*[32] presented discrete fracture-vug network model (DFVN) modeling fluid flow in carbonate rocks. However, to the best of my knowledge, reliable characterization of actual pore networks in acidized region is severely limited, and the corresponding analytical models for acidizing wells with wormholes are scarce. In 2014, Wang *et al.*[33] derived a theoretical model considering acid wormholes to recognize the flow characteristics. And in their model, the pore networks in acidized region were conceptualized as multi-branched wormholes (i.e., the pore networks in acidized region were simplified as multi-branched high-permeability channels), which were used to bridge the gap between the outer region of triple medium and the wellbore. In 2018, Wang *et al.*[34] also investigated flow characteristics in fractured-vuggy carbonate reservoirs using semi-analytical model considering wormholes as multi-branched fractures. Other scholars proposed composite model to study the pressure transient characteristics in fractured-vuggy reservoirs within which the pore networks in acidized region are equivalent to homogeneous medium of Euclidean geometry[35,36]. Generally speaking, due to the interaction and connectivity between the wormholes and the matrix-fracture-vug systems, the acidized region with multiple property scales and non-Euclidean pore network[37] was highlighted by the characteristics of heterogeneity, which increases the research complexity. As a result, developing an applicable analytical model solving this challenge is more desirable.

It is reported that reservoir heterogeneity provides uncertainty in fluid flow through porous media, so, in order to provide a more realistic representation of flow in acidized fractured-vuggy reservoirs, the heterogeneity of the pore networks in acidized region should be taking into consideration. However, previous models neglect the heterogeneity in acidized region. In this paper, we derive an analytical solution by considering the heterogeneity of the pore networks in acidized region to analyze flow characteristic in fractured-vuggy carbonate reservoirs. In this presented model, pore networks properties (porosity and permeability) in acidized region recognized as an inner zone is modeled based on the fractal geometry theory. The schematic diagram of the physical model is shown in Fig. 1. Compared with the previous models, our model takes the heterogeneity of the pore networks in acidized region into account. The derived model can help to reduce the uncertainty in flow through porous media and obtain data with high accuracy.

As the outline of this work, the theoretical models and the corresponding analytical solution in Laplace space are provided in the following section. Then, the results will be analyzed, followed by the discussions of the derived model. Finally, the conclusions are presented.

Methods

Physical concept. As observed in the carbonate formation of the Tahe and Tarim Oilfield in western China, fractured-vuggy reservoirs typically consist of matrix, fracture and vug systems[5]. It is reported that acidizing or acid fracturing stimulation technology has become an important stimulation measure, which is essential to improve or recover productivity for fractured-vuggy carbonate reservoirs[13,38,39]. During the process of acidizing, wormhole dissolution patterns will be affected by a series of complicated physical chemical transportations and reactions[40,41]. As shown in Fig. 2 (i.e. the schematic of the fractured-vuggy model), the physical model was conceptualized as a composite model, which could be divided into the acidized region (interior region) and outer region. In the acidized region, the complicated wormholes are usually connected with matrix-vug-fracture system which is treated as a fractal medium. And the outer region is treated as a common triple medium[29,31,42]. Using the conceptual model, the new composite model is derived under the following assumptions:

(1) As fractal geometry theory is a natural candidate for the representation of heterogeneity of the acidized region[43–45], fractal geometry theory is applied in this article to account for the pore network in the acidized region. However, the outer region is assumed as a common triple medium, in which matrix and vug are regarded as the main sources of hydrocarbon, and fracture is treated as the flow path[35,46]. The formation effective thickness is constant.
(2) During the flow, the property parameters, such as permeability, porosity and fluid viscosity, are constant. Gravity is neglected. Moreover, the isothermal and Darcy flow process is assumed.

Mathematical model. As depicted in Fig. 3, the composite model can be divided into the acidized region (interior region) and outer region. Based on fractal geometry theory, the permeability and porosity in the interior region can be expressed as[47–49]

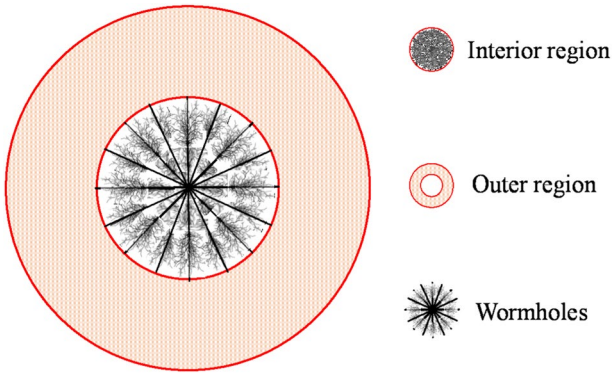

Figure 2. Schematic of the fractured-vuggy physical model.

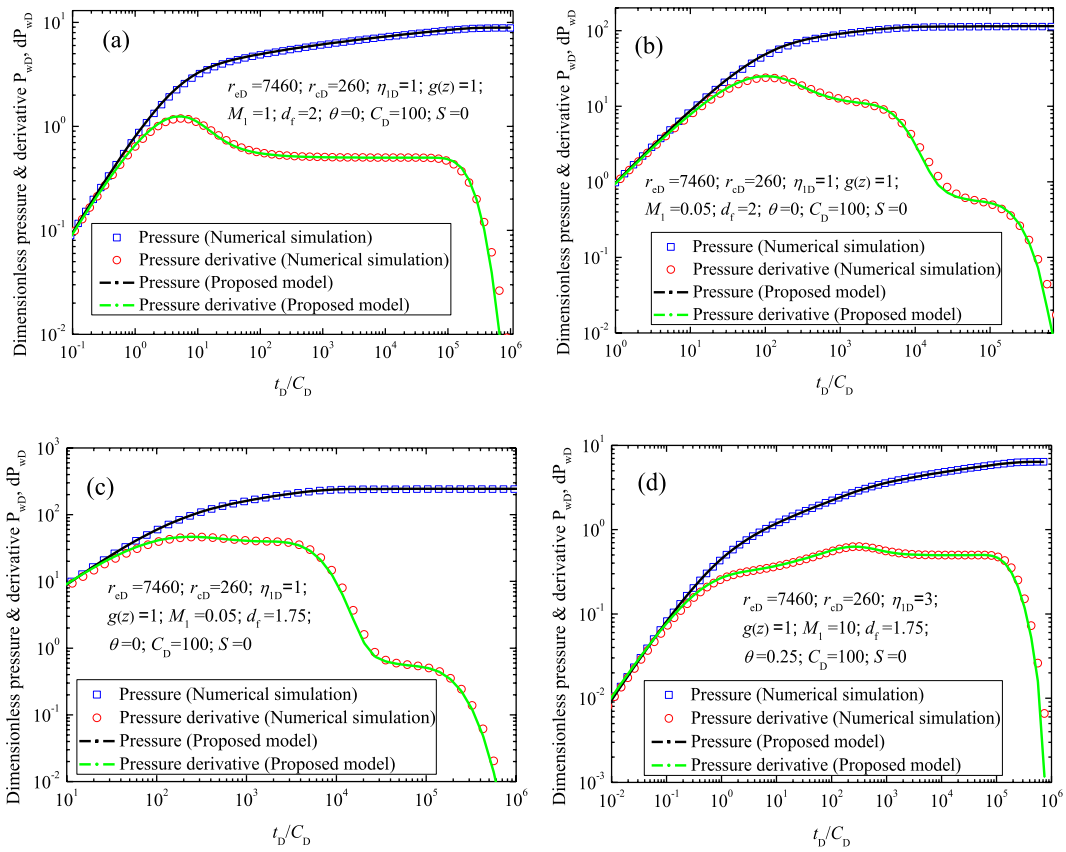

Figure 3. Comparison of P_{wD} and dP_{wD} obtained from the proposed model and numerical simulation: (**a**) case 1; (**b**) case 2; (**c**) case 3; (**d**) case 4.

$$k = k_1\left(\frac{r}{r_w}\right)^{d_f-\theta-2} \quad ; \quad \varphi = \varphi_1\left(\frac{r}{r_w}\right)^{d_f-2} \tag{1}$$

where k_1 is the permeability at the edge of the wellbore, φ_1 is porosity at the edge of the wellbore, r_w is wellbore radius, d_f is pore spaces fractal dimension, θ is the conductivity index[49,50].

Based on Eq. (1), the corresponding governing equation in interior region is

$$\frac{\partial^2 p_1}{\partial r^2} + \frac{d_f-\theta-1}{r}\frac{\partial p_1}{\partial r} = \frac{C_t\mu\varphi_1}{k_1}\left(\frac{r}{r_w}\right)^{\theta}\frac{\partial p_1}{\partial t} \quad (r_w \le r \le r_c) \tag{2}$$

in which p_1 is the pressure in interior region, μ is the fluid viscosity, C_t is the rock compressibility in interior region, r_c is the outer boundary of the acidized region, and t is the time.

In outer region, the corresponding governing equation can be given by

$$\begin{cases} \frac{k_F}{\mu}\frac{1}{r}\frac{\partial}{\partial r}\left(r\frac{\partial p_F}{\partial r}\right) - C_M\varphi_M\frac{\partial p_M}{\partial t} - C_v\varphi_v\frac{\partial p_v}{\partial t} = C_F\varphi_F\frac{\partial p_F}{\partial t} & (r_c \le r \le r_e) \\ C_M\varphi_M\frac{\partial p_M}{\partial t} = \frac{\alpha_{FM}k_M}{\mu}(p_F - p_M) & (r_c \le r \le r_e) \\ C_v\varphi_v\frac{\partial p_v}{\partial t} = \frac{\alpha_{Fv}k_v}{\mu}(p_F - p_v) & (r_c \le r \le r_e) \end{cases} \tag{3}$$

where r_e is the outer boundary of the reservoir, the subscript F, M and v represent the fracture system, matrix system and vug system. k_τ (τ = F, M and v) is the permeability in outer region. p_τ (τ = F, M and v) is the pressure in outer region. φ_M is matrix porosity, φ_F is fracture porosity and φ_v is vug porosity. C_M is matrix compressibility, C_F is fracture compressibility and C_v is vug compressibility. α_{FM} and α_{Fv} are shape factors for fracture-vug and fracture-matrix, respectively. More details about the calculation equations for physical parameters in triple medium, such as k_F, k_v, φ_F, φ_v, α_{FM} and α_{Fv}, can be found in Appendix A.

At the initial state, the following pressure equation can be written as

$$p_F(r, t = 0) = p_M(r, t = 0) = p_v(r, t = 0) = p_0 \tag{4}$$

where p_0 is the initial pressure.

Three types of external boundary conditions (constant pressure boundary, infinite boundary or closed boundary) can be expressed respectively as[5]

$$p_F(r = r_e, t) = p_0 \tag{5a}$$

$$p_F(r = r_e \to \infty, t) = p_0 \tag{5b}$$

$$\left.\frac{\partial p_F}{\partial r}\right|_{r=r_e} = 0 \tag{5c}$$

The inner boundary condition can be expressed as

$$\left.\frac{2\pi k_1 h}{\mu}\left(r\frac{\partial p_1}{\partial r}\right)\right|_{r=r_w} = qB \tag{6}$$

where h is effective thickness, B is fluid volume factor, and q is the flow rate at wellhead, which is positive for producers and negative for injectors.

The interface continuity conditions are governed by

$$\begin{cases} p_1|_{r=r_c} = p_F|_{r=r_c} \\ \left.\frac{k_1}{\mu}\left(\frac{r_c}{r_w}\right)^{d_f-\theta-2}\frac{\partial p_1}{\partial r}\right|_{r=r_c} = \left.\frac{k_F}{\mu}\frac{\partial p_F}{\partial r}\right|_{r=r_c} \end{cases} \tag{7}$$

By using dimensionless variables listed in Table 1, Eqs (2–7) can be rewritten as following:

$$\begin{cases} \frac{\partial^2 p_{1D}}{\partial r_D^2} + \frac{d_f - \theta - 1}{r_D}\frac{\partial p_{1D}}{\partial r_D} = \frac{\eta_{1D}}{M_1}r_D^\theta\frac{\partial p_{1D}}{\partial t_D} \\ \frac{1}{r_D}\frac{\partial}{\partial r_D}\left(r_D\frac{\partial p_{FD}}{\partial r_D}\right) - \lambda_{FM}(p_{FD} - p_{MD}) - \lambda_{Fv}(p_{FD} - p_{vD}) = \eta_{FD}\frac{\partial p_{FD}}{\partial t_D} \\ \eta_{MD}\frac{\partial p_{MD}}{\partial t_D} = \lambda_{FM}(p_{FD} - p_{MD}); \quad \eta_{vD}\frac{\partial p_{vD}}{\partial t_D} = \lambda_{Fv}(p_{FD} - p_{vD}) \\ p_{FD}(r_D, t_D = 0) = p_{MD}(r_D, t_D = 0) = p_{vD}(r_D, t_D = 0) = 0 \\ p_{FD}(r_D = r_{eD}, t_D) = 0; \quad \text{or } p_{FD}(r_D = r_{eD} \to \infty, t_D) = 0; \quad \text{or } \left.\frac{\partial p_{FD}}{\partial r_D}\right|_{r_D=r_{eD}} = 0 \\ \left.\frac{\partial p_{1D}}{\partial r_D}\right|_{r_D=1} = -\frac{1}{M_1}; \quad p_{1D}|_{r_D=r_{cD}} = p_{FD}|_{r_D=r_{cD}}; \quad M_1 r_{cD}^{d_f-\theta-2}\left.\frac{\partial p_{1D}}{\partial r_D}\right|_{r_D=r_{cD}} = \left.\frac{\partial p_{FD}}{\partial r_D}\right|_{r_D=r_{cD}} \end{cases} \tag{8}$$

Defined parameters	Expressions
Dimensionless time, t_D	$t_D = k_F t / \left[\left(\varphi_M C_M + \varphi_F C_F + \varphi_v C_v\right)\mu r_w^2\right]$
Dimensionless pressure, p_D	$p_D = 2\pi k_F h(p_0 - p)/(qB\mu)$
Dimensionless radius, r_D	$r_D = r/r_w$
Diffusivity ratio between the two regions, η_{1D}	$\eta_{1D} = C_{t1}\varphi_1 / \left(\varphi_M C_M + \varphi_F C_F + \varphi_v C_v\right)$
Fracture storage capacitance coefficient, η_{FD}	$\eta_{FD} = C_F\varphi_F / \left(\varphi_M C_M + \varphi_F C_F + \varphi_v C_v\right)$
Matrix storage capacitance coefficient, η_{MD}	$\eta_{MD} = C_M\varphi_M / \left(\varphi_M C_M + \varphi_F C_F + \varphi_v C_v\right)$
Vug storage capacitance coefficient, η_{vD}	$\eta_{vD} = C_v\varphi_v / \left(\varphi_M C_M + \varphi_F C_F + \varphi_v C_v\right)$
Permeability ratio, M_1	$M_1 = k_1/k_F$
Fracture-matrix inter-porosity coefficient, λ_{FM}	$\lambda_{FM} = \alpha_{FM} r_w^2 k_M / k_F$
Fracture-vug inter-porosity coefficient, λ_{Fv}	$\lambda_{Fv} = \alpha_{Fv} r_w^2 k_v / k_F$

Table 1. Summary of the variables in the model.

Cases	Parameters							
	r_{eD}	r_{cD}	C_D	S	d_f	θ	η_{1D}	M_1
1	7460	260	100	0	2	0	1	1
2	7460	260	100	0	2	0	1	0.05
3	7460	260	100	0	1.75	0	1	0.05
4	7460	260	100	0	1.75	0.25	3	10

Table 2. Synthetic data used for validation.

Based on the derived process stated in Appendix B, the analytical solution for Eq. (8) in Laplace space can be obtained. The wellbore pressure in Laplace space considering the wellbore storage and the skin effects is

$$\bar{P}_{wD} = \frac{z[AI_n(\beta) + BK_n(\beta)] + S}{z[1 + C_D z(z[AI_n(\beta) + BK_n(\beta)] + S)]} \tag{9}$$

where S is the skin factor, C_D is the dimensionless wellbore storage coefficient. Then, with the Stehfest inversion algorithm[51], the wellbore pressure in real space can be obtained.

Results

Validation of the proposed model. To validate the derived analytical solution, the dimensionless pressure and derivative (P_{wD} and dP_{wD}) of the new derived model are compared with numerical solutions. In the calculation, the outer boundary condition is set as constant pressure, and the function $g(z)$ in Eq. (11) is set to be 1 (the outer region of the model can be simplified as the homogeneous porous media). Table 2 summarizes the data used for the comparison. Result (Fig. 3) illustrates that calculations from the proposed model agree well with those from numerical simulation.

Comparison with former models. When parameters d_f, θ and $g(z)$ in our derived model are assigned as 2, 0 and 1, respectively, the acidized region (inner region) can be considered homogeneous, and the reservoir can be regarded as two different but uniform regions. In this case, our derived model can be validated with radial composite model. Figure 4a presents the comparison of the results (P_{wD} versus t_D) from the derived model and that from fractal radial composite model proposed by Razminia *et al.*[52] When parameters d_f and θ in fractal radial composite model are set to be 2 and 0, respectively, fractal radial composite model can be simplified as the conventional radial composite model. In the calculation, the outer boundary condition is set as infinite boundary, other parameters applied in the model assigned were: $C_D = 200$, $S = 2$ and $r_{cD} = 500$. Results (Fig. 4a) suggest that the derived model is validated. When parameters d_f, θ, M_1, η_{1D}, and $g(z)$ in our derived model are assigned as 2, 0, 1, 1 and 1, respectively, the reservoir can be regarded as a homogeneous porous media. In this case, the derived model can be compared with the classic radial flow model derived by Agarwal *et al.*[53] Fig. 4b presents the comparison of the results (P_{wD} versus t_D) from the derived model and that from the classic analytical solution[53]. In the calculation, the outer boundary condition is set as infinite boundary, other parameters applied in the model assigned were: $C_D = 200$ and $S = 2$. Results (Fig. 4b) also suggest that the derived model is validated. Figure 4a,b show the former classic models are special cases of the new derived model, and the new derived analytical model can be used to analyze more complex flow behaviors.

Flow characteristic curves. As stated in the literatures[5,33], the flow characteristic curves can be used for recognizing flow behavior in the reservoir. Taking the closed outer boundary condition as example, the flow characteristic curve will be discussed in detail. Figure 5a presents the log-log curves (i.e., t_D versus P_{wD} and dP_{wD}) for closed outer boundary condition. In the calculation, fractal dimension of the pore spaces d_f is 2, the conductivity index θ is 0, the dimensionless parameters r_{eD} and r_{cD} are 30000 and 2000, respectively, skin factor S assigned is

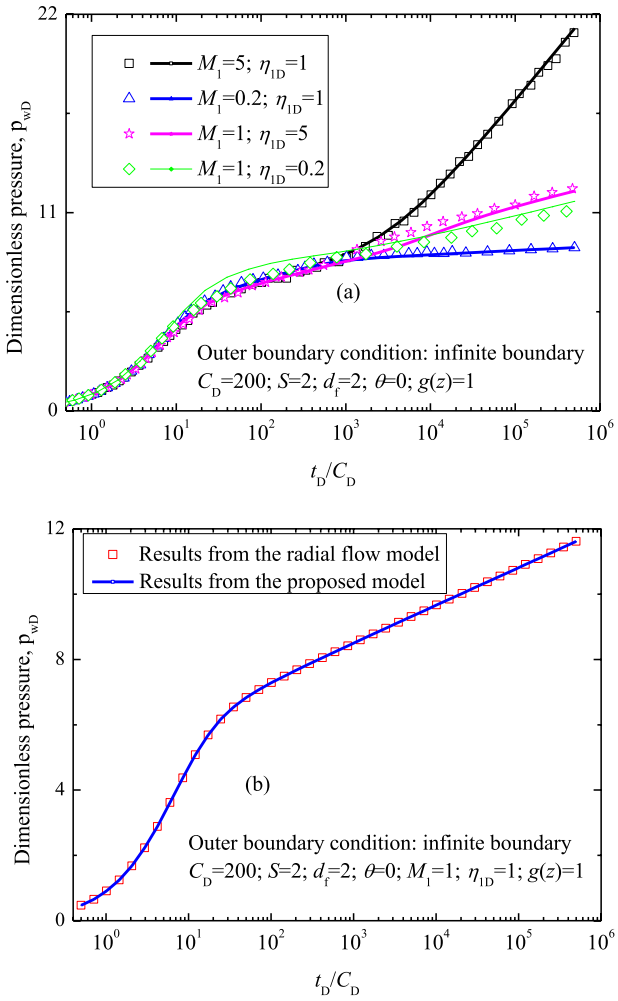

Figure 4. Comparison of P_{wD} obtained from the proposed model and other models: (**a**) for radial composite model; (**b**) for radial model. Results from former models are shown with points, and calculations from the derived model are solid lines.

0, C_D assigned is 200, diffusivity ratio between the two regions η_{1D} is 0.127, fracture storage capacitance coefficient η_{FD} is 0.022, matrix storage capacitance coefficient η_{MD} is 0.106, vug storage capacitance coefficient η_{vD} is 0.872, permeability ratio M_1 is 1.251, λ_{FM} assigned is 2.01×10^{-7}, and λ_{Fv} assigned is 9.70×10^{-3}. With the same parameters, Fig. 5b compares the differences of three well testing curves to study the effect of outer boundary on flow characteristics. Results (Fig. 5a,b) illustrate that the flow characteristic curves can be characterized by six flow stages:

The first stage is well storage stage, in which the fluid flow is dominated by the parameters S and C_D.

The second stage is radial flow in the inner region. The dP_{wD} curve shows zero slope horizontal line. During this period, the fluid in the interior region flows into the wellbore. The flow characteristic is mainly controlled by the parameters r_{cD}, pore spaces fractal dimension and the conductivity index. The larger the range of the inner region is, the longer the stage 2 will be.

The third stage is fracture-vug inter-porosity flow stage, in which the dP_{wD} curve shows the first concave. The concave shape represents the supplement between the fracture system and vug system. In this stage, the pressure wave has propagated to the coupling interface, and the flow characteristic in this period is mainly controlled by fracture-vug inter-porosity coefficient.

The fourth stage is transition flow stage, which presents a straight line with the slope 0.5 on the log-log curve of t_D versus dP_{wD}.

The fifth stage is fracture-matrix inter-porosity flow stage, in which the dP_{wD} curve shows the second concave shape. The second concave shape segment reflects supplement from matrix to fracture. During this stage, flow characteristic is mainly controlled by fracture-matrix inter-porosity coefficient.

The sixth stage is external boundary response stage, in which flow characteristic in the reservoir is mainly controlled by the parameter r_{eD}.

Sensitivity analysis. In this part, we will study the influences of parameters on well testing curves in detail. The outer boundary is set as closed pressure, the parameter values is listed in Table 3. The presented model

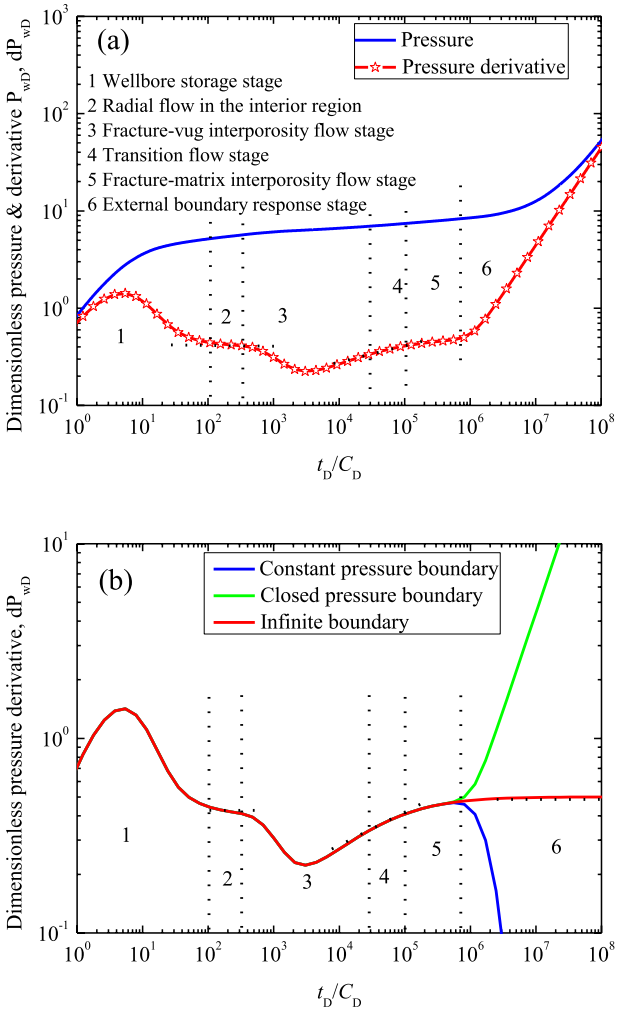

Figure 5. Flow characteristic curves: (**a**) pressure & pressure derivative curves for closed boundary condition; (**b**) pressure derivative curves for three different outer boundary conditions.

Parameter	Parameter value	Parameter	Parameter value
φ_M	0.1	r_{eD}	30000
r_w/m	0.1	r_{cD}	2000
L_M/m	2	η_{1D}	0.127
L_F/m	8×10^{-4}	η_{FD}	0.022
L_v/m	1.08	η_{MD}	0.106
k_1/m^2	1.0×10^{-10}	η_{vD}	0.872
K_M/m^2	1.6×10^{-14}	λ_{FM}	2.01×10^{-7}
d_f	2	λ_{Fv}	9.66×10^{-3}
θ	0	M_1	1.56

Table 3. Parameter values.

demonstrates that d_f, θ, r_c, L_M, L_F and L_v are the basic parameters, which can determine the flow characteristic in acidized fractured-vuggy reservoirs. The basic parameters and their ranges used for sensitivity analysis are summarized in Table 4.

Figure 6 shows flow characteristic curves with different inner region parameters (i.e., inner region fractal dimension, inner region connectivity index and inner region radius). Figure 6a presents the effect of parameter d_f on the flow characteristic curves (for $1.65 \le d_f \le 2$). As shown in Fig. 6a, P_{wD} and dP_{wD} in stages 1, 2 and 3 decrease with the increased inner region fractal dimension d_f. This can be interpreted as that the larger inner region fractal dimension d_f implies inner region permeability increasing, leading to the decrease of flow resistance and the dimensionless pressure. Figure 6b demonstrates the effect of inner region connectivity index θ on the flow

Parameter	Range of the parameter	Parameter	Range of the parameter
d_f	$1.65 \le d_f \le 2$	L_M/m	$1.5 \le L_M \le 2.5$
θ	$-0.25 \le \theta \le 0.25$	L_F/m	$3 \times 10^{-4} \le L_F \le 8 \times 10^{-4}$
r_c/m	$100 \le r_c \le 300$	L_v/m	$0.8 \le L_v \le 1.2$

Table 4. Ranges of parameters for sensitivity analysis.

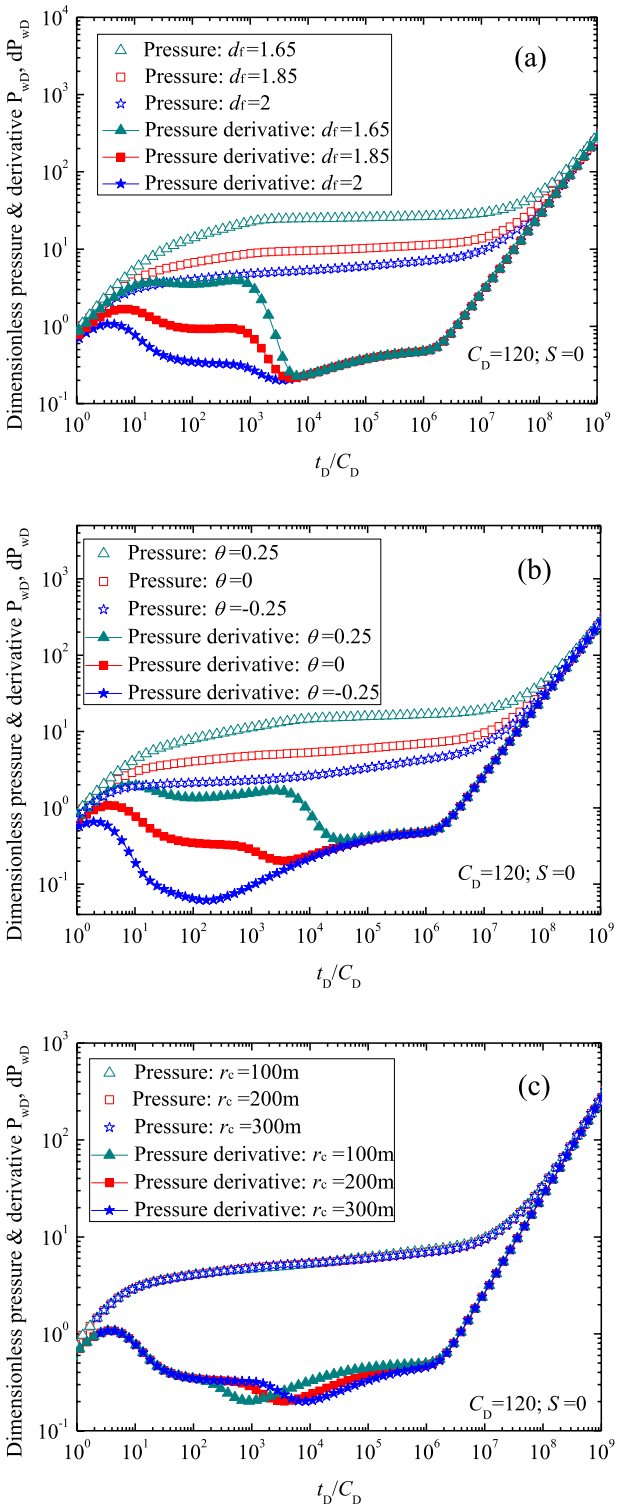

Figure 6. Effects of parameters of inner region on the well testing curves: (**a**) for inner region fractal dimension; (**b**) for inner region connectivity index; (**c**) for parameter r_c.

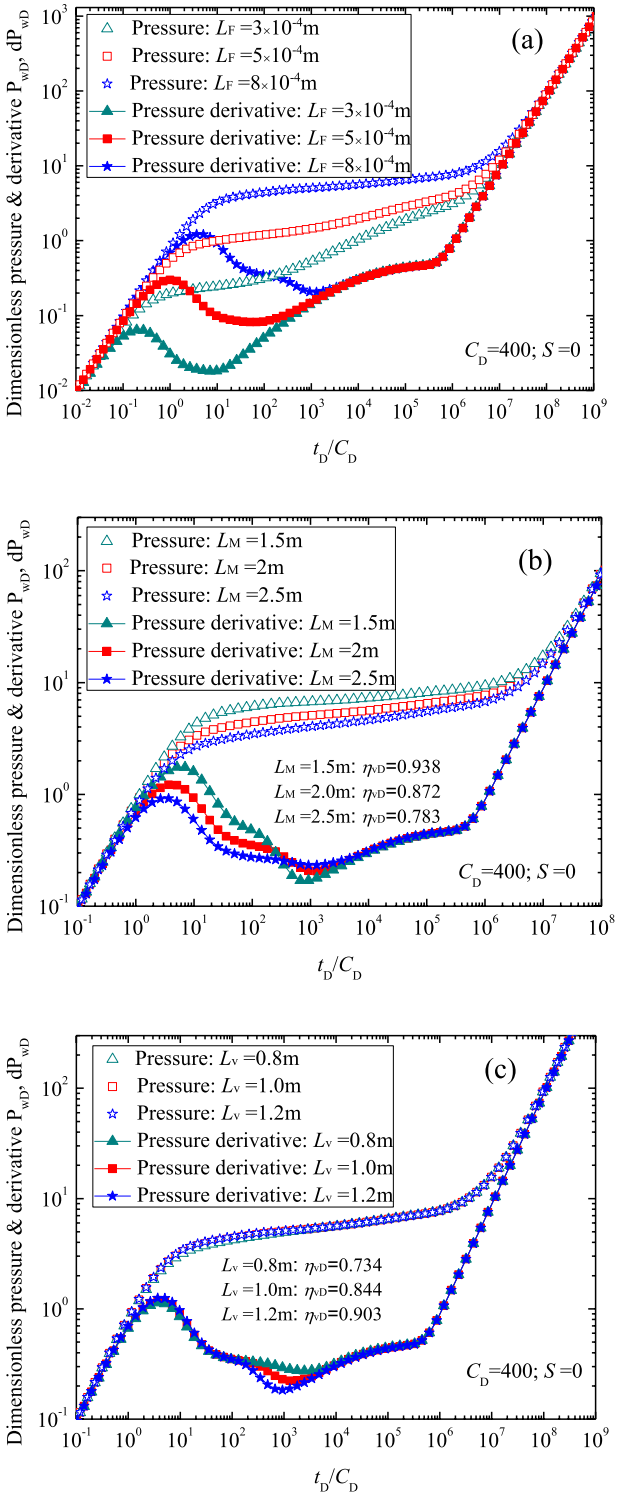

Figure 7. Effect of basic parameters in outer region on the dimensionless wellbore pressure: (**a**) for the space interval of fracture in outer region; (**b**) for the matrix block size in outer region; (**c**) for the radius of the vug in outer region.

characteristic curves (for $-0.25 \le \theta \le 0.25$). Figure 6b demonstrates P_{wD} and dP_{wD} in stages 1, 2 and 3 increase with the increased inner region connectivity index θ. Figure 6c illustrates the effect of inner region radius on the flow characteristic curves (for $100\,m \le r_c \le 300\,m$). Results (Fig. 6c) show P_{wD} and dP_{wD} in stages 3 to 5 decrease with the increased inner region radius. The main reason for this is the permeability at the edge of the wellbore k_1 is larger than fracture system permeability k_F ($M_1 > 1$). Figure 6c also shows a longer period of radial flow (stage 2) corresponds to a larger inner region radius, which is expected. Figure 6 demonstrates that forming larger acidized region can help improve well production and reduce fluid pressure loss.

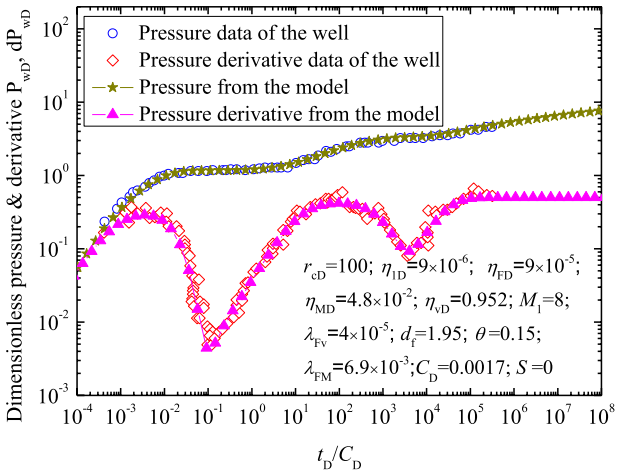

Figure 8. Comparison of the calculated results with actual test data.

Figure 7 presents the influences of the outer region parameters, such as the space interval of fracture system L_F, matrix block size L_M and radius of the vug L_v, on the transient pressure behavior. Figure 7a presents the effect of the space interval of fracture system L_F on the flow characteristic curves (for $3 \times 10^{-4}\,\text{m} \le L_F \le 8 \times 10^{-4}\,\text{m}$). As shown in Fig. 7a, a larger L_F corresponds to a larger pressure depletion. The main reason is that a greater parameter L_F value results in a smaller parameter M_1 and the smaller parameter η_{1D}. We can see that the effect of parameter L_F on the well testing curves is concentrated in stages 1 to 4. Figure 7b demonstrates the effect of matrix block size in outer region on the flow characteristic curves (for $1.5\,\text{m} \le L_M \le 2.5\,\text{m}$). We can see that P_{wD} in stages 1 to 4 decreases with the increasing matrix block size L_M. As a larger L_M corresponding to a larger M_1, which leads to a smaller pressure depletion in stages 1 and 2. Furthermore, parameter η_{vD} decreases as parameter L_M increases, indicating the supplement of the vug system to fracture system decreases will the increasing parameter L_M. As a result, the dimensionless pressure derivation in stage 3 increases with the increasing L_M. Figure 7c shows the effect of parameter L_v in outer region on the flow characteristic curves (for $0.5\,\text{m} \le L_v \le 1.2\,\text{m}$). It can be seen that the effects of L_v on P_{wD} and dP_{wD} curves are concentrated in stage 3, where a larger L_v will lead to a smaller pressure depletion. The main reason is that, a larger L_v implies larger energy in the vugs, leading to increased supply from the vug system to the fracture system, which makes the pressure derivative values smaller.

Case example. In this case, pressure transient data from an acidized well in Tahe oilfield (Tarim basin, China), is selected to interpret. The actual test data of the acidized well are cited from Wang *et al.*[33]. In the calculation, the parameters measured are P_{wD} and dP_{wD} and the corresponding t_D, and the fitting parameters mainly concludes: d_f; θ; r_{cD}; η_{1D}; η_{FD}; η_{MD}; η_{vD}; M_1; λ_{Fv}; λ_{FM}; C_D and S. Figure 8 presents the fitting results and the actual test data, and the corresponding results by well test interpretation are as follows: $d_f = 1.95$; $\theta = 0.15$; $r_{cD} = 100$; $\eta_{1D} = 9 \times 10^{-6}$; $\eta_{FD} = 9 \times 10^{-5}$; $\eta_{MD} = 4.8 \times 10^{-2}$; $\eta_{vD} = 0.952$; $M_1 = 8$; $\lambda_{Fv} = 4 \times 10^{-5}$; $\lambda_{FM} = 6.9 \times 10^{-3}$; $C_D = 0.0017$; $S = 0$. Figure 8 illustrates that the results agree with each other, which verifies the presented model.

Discussions

Advantages and limitations of the derived model. The analytical model lays theoretical foundations for characterizing the flow characteristic curves and dynamic pressure of acidized well in acidized carbonate porous media. With this new analytical solution, it can help to reduce the uncertainty in flow through porous media and obtain data with high accuracy. In addition, it can be applied to field case study and estimate more accurate reservoir parameters reflecting flow characteristic using inverse modeling. However, it should be noted that the derived model is limited to single-phase flow. Multi-phase fluid flow in fractured-vuggy carbonate porous medium is an interesting and challenging topic, and the corresponding work is still under processing.

Conclusions

Based on fractal theory and triple medium concept model, a novel analytical solution to a fractal composite model is derived to study the flow characteristic in acidized carbonate reservoirs. Predicted results deduced from the derived analytical solution agree well with numerical simulation results. For the closed outer boundary condition, the influence of basic parameters, such as d_f, θ, r_c, L_M, L_F and L_v, on flow characteristic curves are studied in detail. Followings are the main conclusions:

1. The calculated results (both P_{wD} and d P_{wD}) based on the derived analytical solution match the actual test data very well, which illustrates this proposed model can be applied to field case study.
2. As the inner region permeability is larger than fracture system permeability, forming larger acidized region can help improve well production and reduce fluid pressure loss.
3. The new analytical solution to the fractal composite model, considering the heterogeneity of the pore networks in acidized region, is useful for flow characteristic analysis of acidized well in acidized carbonate

porous media. With this new analytical solution, it can help to reduce the uncertainty in flow through porous media and obtain data with high accuracy. In addition, it can be applied to estimate more accurate reservoir parameters reflecting flow characteristic using inverse modeling.

References

1. Kossack, C. A., Gurpinar, O. A methodology for simulation of vuggy and fractured reservoirs. Paper SPE-66366-MS presented at the SPE Reservoir Simulation Symposium, Houston, Texas, 11–14 February (2001).
2. Rivas-Gomez, S. *et al*. Numerical simulation of oil displacement by water in a vuggy fractured porous medium. Paper SPE-66386-MS presented at SPE Reservoir Simulation Symposium, Houston, Texas, 11–14 February (2001).
3. Camacho-Velazquez, R. *et al*. Pressure transient and decline curve behaviors in naturally fractured vuggy carbonate reservoirs. Paper SPE-77689-MS presented at SPE Annual Technical Conference and Exhibition, San Antonio, Texas, 29 September-2 October (2002).
4. Kang, Z. J. *et al*. Percolation characteristics of fractured-vuggy carbonate reservoir in Tahe oilfield. *Oil Gas Geol.* **26**(5), 634–640 (2005).
5. Gao, B. *et al*. Pressure transient analysis of a well penetrating a filled cavity in naturally fractured carbonate reservoirs. *Journal of Petroleum Science and Engineering* **145**, 392–403 (2016).
6. Lyu, X. *et al*. Mechanism and influencing factors of EOR by N2 injection in fractured-vuggy carbonate reservoirs. *Journal of Natural Gas Science and Engineering* **40**, 226–235 (2017).
7. Fuentes-Cruz, G., Camacho-Velazquez, R. & Vásquez-Cruz, M. Pressure transient and decline curve behaviors for partially penetrating wells completed in naturally fractured-vuggy reservoirs. Paper SPE-92116-MS presented at SPE International Petroleum Conference in Mexico, 7–9 November (2004).
8. Jia, Y. L. *et al*. Flow modeling of well test analysis for porous–vuggy carbonate reservoirs. *Transport in Porous Media* **97**(2), 253–279 (2013).
9. Guo, J. C., Nie, R. S. & Jia, Y. L. Dual permeability flow behavior for modeling horizontal well production in fractured-vuggy carbonate reservoirs. *Journal of hydrology* **464**, 281–293 (2012).
10. Popov, P. *et al*. Multiphysics and multiscale methods for modeling fluid flow through naturally fractured carbonate karst reservoirs. *SPE Reservoir Evaluation & Engineering* **12**(2), 218–231 (2009).
11. Rzonca, B. Carbonate aquifers with hydraulically non-active matrix: a case study from Poland. *Journal of hydrology* **355**(1), 202–213 (2008).
12. Huang, T. P., Hill, A. D. & Schechter, R. S. Reaction rate and fluid loss: the key to wormhole initiation and propagation in carbonate acidizing. Presented at International Symposium on Oilfield Chemistry, 18–21 February, Houston, Texas, SPE-37312-MS (1997).
13. Qiu, X. *et al*. Quantitative modeling of acid wormholing in carbonates-what are the gaps to bridge. Paper SPE-164245-MS presented at SPE Middle East Oil and Gas Show and Conference (2013).
14. Kang, Q. *et al*. Lattice Boltzmann simulation of chemical dissolution in porous media. *Physical Review E* **65**(3), 036318 (2002).
15. Mostofizadeh, B. & Economides, M. J. Optimum injection rate from radial acidizing experiments. Paper SPE-28547-MS presented at SPE Annual Technical Conference and Exhibition, New Orleans, Louisiana, 25–28 September (1994).
16. Frick, T. P., Mostofizadeh, B. & Economides, M. J. Analysis of radial core experiments for hydrochloric acid interaction with limestones. Paper SPE-27402-MS presented at SPE Formation Damage Control Symposium, Lafayette, Louisiana, 7–10 February (1994).
17. Fredd, C. N. Dynamic model of wormhole formation demonstrates conditions for effective skin reduction during carbonate matrix acidizing. Paper SPE-59537-MS presented at SPE Permian Basin Oil and Gas Recovery Conference, Midland, 21–23 March (2000).
18. Tremblay, B. Modelling of sand transport through wormholes. *Journal of Canadian Petroleum Technology* **44**(4), 51–58 (2005).
19. Liu, M. *et al*. Wormhole propagation behavior under reservoir condition in carbonate acidizing. *Transport in Porous Media* **96**(1), 203–220 (2013).
20. Zakaria Mohamed Reda A. Tracer fluid flow through porous media: theory applied to acid stimulation treatments in carbonate rocks. PhD thesis, Texas A. & M. University (2014).
21. Li, X. *et al*. Large-scale visual experiment and numerical simulation of acid fingering during carbonate acid fracturing. Paper SPE-187019-MS presented at SPE/IATMI Asia Pacific Oil & Gas Conference and Exhibition, Jakarta, Indonesia, 17–19 October (2017).
22. Dejam, M., Hassanzadeh, H. & Chen, Z. Shear dispersion in a fracture with porous walls. *Advances in water resources* **74**, 14–25 (2014).
23. Dejam, M., Hassanzadeh, H. & Chen, Z. Shear dispersion in a capillary tube with a porous wall. *Journal of contaminant hydrology*, 2016, **185**, 87–104 (2016).
24. Dejam, M., Hassanzadeh, H. & Chen, Z. A reduced-order model for chemical species transport in a tube with a constant wall concentration. *The Canadian Journal of Chemical Engineering* **96**(1), 307–316 (2018).
25. Dejam, M. Dispersion in non-Newtonian fluid flows in a conduit with porous walls. *Chemical Engineering Science* **189**, 296–310 (2018).
26. Dejam, M., Hassanzadeh, H. & Chen, Z. Shear dispersion in a rough-walled fracture. *SPE Journal* **23**(5), 1669–1688 (2018).
27. Dejam, M. Advective-diffusive-reactive solute transport due to non-Newtonian fluid flows in a fracture surrounded by a tight porous medium. *International Journal of Heat and Mass Transfer* **128**, 1307–1321 (2019).
28. Ugursal, A. Development of acid fracturing model for naturally fractured reservoirs. PhD thesis, Texas A&M University (2018).
29. Wu, Y. S. *et al*. A multiple-continuum approach for modeling multiphase flow in naturally fractured vuggy petroleum reservoirs. Paper SPE-104173-MS presented at International Oil & Gas Conference and Exhibition in China, 5–7 December, Beijing, China (2006).
30. Wu, Y. S. *et al*. A triple-continuum pressure-transient model for naturally fractured vuggy reservoir. Paper SPE-110044-MS presented at SPE Annual Technical Conference and Exhibition, Anaheim, 11–14 Nov. (2007).
31. Wu, Y. S. & Qin, G. A generalized numerical approach for modeling multiphase flow and transport in fractured porous media. *Communications in computational physics* **6**(1), 85–108 (2009).
32. Yao, J., Huang, Z. Q. & Li, Y. Z. Discrete fracture-vug network model for modeling fluid flow in fractured vuggy porous media. Paper SPE-130287-MS presented at International Oil and Gas Conference and Exhibition in China, Beijing, 8–10 June (2010).
33. Wang, L. *et al*. Analytical modeling of flow behavior for wormholes in naturally fractured-vuggy porous media. *Transport in porous media* **105**(3), 539–558 (2014).
34. Wang, L., Chen, X. & Xia, Z. A novel semi-analytical model for multi-branched fractures in naturally fractured-vuggy reservoirs. *Scientific reports* **8**(1), 11586 (2018).
35. Yang, J., Yao, J. & Wang, Z. Study of pressure transient characteristic for triple-medium composite reservoirs. *Journal of Hydrodynamics* **20**(4), 418–425 (2005).
36. Chen, F. *et al*. The flow model of the triple-medium composite reservoirs and the type curves. *Journal of Daqing Petroleum Institute* **32**(6), 67–75 (2008).

37. Yao, Y. D., Wu, Y. S. & Zhang, R. L. The transient flow analysis of fluid in a fractal, double-porosity reservoir. *Transport in porous media* **94**(1), 175–187 (2012).
38. Liu, P. *et al*. Analysis and simulation of rheological behavior and diverting mechanism of in situ self-diverting acid. *Journal of Petroleum Science and Engineering* **132**, 39–52 (2015).
39. Zhang, H. W. *et al*. Dual fractal model of carbonate acidizing wormholes. *Natural Gas Geoscience* **28**(3), 466–472 (2017).
40. Fredd, C. N. & Miller, M. J. Validation of carbonate matrix stimulation models. Paper SPE-58713-MS presented at SPE International Symposium on Formation Damage Control, Lafayette, Louisiana 23–24 February (2000).
41. Liu, M., Zhang, S. C. & Mou, J. Dissolution pattern of radial wormhole model in carbonate acidizing. *Petroleum Geology and Recovery Efficiency* **19**(2), 106–110 (2012).
42. Abdassah, D. & Ershaghi, I. Triple-porosity systems for representing naturally fractured reservoirs. *SPE Formation Evaluation* **1**(2), 113–127 (1986).
43. Li, X. G., Yang, Z. Z. & Su, J. Z. Fractal mathematical model of 3D acid corrosion of rough carbonate rock particles. *Xingjiang Petroleum Geology* **31**(2), 167–170 (2010).
44. Liu, M. *et al*. Fractal nature of acid-etched wormholes and the influence of acid type on wormholes. *Petroleum Exploration and Development* **39**(5), 591–596 (2012).
45. Zhang, H. W. *et al*. Fractal model of carbonate acidizing wormhole and acidizing parameter optimization. *Journal of Southwest Petroleum University (Science & Technology Edition)* **39**(2), 105–110 (2017).
46. Di, Y. *et al*. A method to determine the size limit between dissolution pores and vugs in triple medium. *Journal of Basic Science and Engineering* **21**(4), 692–701 (2013).
47. Acuna, J. A., Ershaghi, I. & Yortsos, Y. C. Practical application of fractal pressure transient analysis of naturally fractured reservoirs. *SPE Formation Evaluation* **10**(3), 173–179 (1995).
48. Wang, W., Shahvali, M. & Su, Y. A semi-analytical fractal model for production from tight oil reservoirs with hydraulically fractured horizontal wells. *Fuel* **158**, 612–618 (2015).
49. Cossio, M., Moridis, G. & Blasingame, T. A. A semianalytic solution for flow in finite-conductivity vertical fractures by use of fractal theory. *SPE Journal* **18**(1), 83–96 (2013).
50. Chang, J. & Yortsos, Y. C. Pressure transient analysis of fractal reservoirs. *SPE Formation Evaluation* **5**(1), 31–38 (1990).
51. Stehfest, H. Algorithm 368: numerical inversion of laplace transforms [D5]. *Communications of the ACM* **13**(1), 47–49 (1970).
52. Razminia, K., Razminia, A. & Trujilo, J. J. Analysis of radial composite systems based on fractal theory and fractional calculus. *Signal Processing* **107**, 378–388 (2015).
53. Agarwal, R. G., Al-Hussainy, R. & Ramey, H. J. Jr. An investigation of wellbore storage and skin effect in unsteady liquid flow: I. Analytical treatment. *Society of Petroleum Engineers Journal* **10**(03), 279–290 (1970).

Acknowledgements

The authors are grateful for financial support from the Deanship of Scientific Research at King Fahd University of Petroleum and Minerals (Project No. SB181033), and the National Natural Science Foundation of China (Grant No. 51604013).

Author Contributions

Gang Lei derived the theoretical model and wrote the main manuscript. Qinzhuo Liao and Dongxiao Zhang supervised the project, discussed the results and revised the manuscript.

Additional Information

Supplementary information accompanies this paper at https://doi.org/10.1038/s41598-019-44802-2.

Competing Interests: The authors declare no competing interests.

Publisher's note: Springer Nature remains neutral with regard to jurisdictional claims in published maps and institutional affiliations.

Open Access This article is licensed under a Creative Commons Attribution 4.0 International License, which permits use, sharing, adaptation, distribution and reproduction in any medium or format, as long as you give appropriate credit to the original author(s) and the source, provide a link to the Creative Commons license, and indicate if changes were made. The images or other third party material in this article are included in the article's Creative Commons license, unless indicated otherwise in a credit line to the material. If material is not included in the article's Creative Commons license and your intended use is not permitted by statutory regulation or exceeds the permitted use, you will need to obtain permission directly from the copyright holder. To view a copy of this license, visit http://creativecommons.org/licenses/by/4.0/.

© The Author(s) 2019